Inorganic Chemistry

pubs.acs.org/IC Article

Strong Magnetocaloric Coupling in Oxyorthosilicate with Dense Gd^{3+} Spins

Ziyu W. Yang, Jie Zhang, Dabiao Lu, Xiaoxiao Zhang, Haoting Zhao, Hongzhi Cui,* Yu-Jia Zeng,* and Youwen Long*

Cite This: *Inorg. Chem.* 2023, 62, 5282−5291 Read Online

ACCESS | Metrics & More | Article Recommendations | Supporting Information

ABSTRACT: Searching for working refrigerant materials is the key element in the design of magnetic cooling devices. Herein, we report on the thermodynamic and magnetocaloric parameters of an X_1 phase oxyorthosilicate, Gd_2SiO_5, by field-dependent static magnetization and specific heat measurements. An overall correlation strength of $|J|S^2 \approx 3.4$ K is derived via the mean-field estimate, with antiferromagnetic correlations between the ferromagnetically coupled Gd−Gd layers. The magnetic entropy change $-\Delta S_m$ is quite impressive, reaches 0.40 J K^{-1} cm^{-3} (58.5 J K^{-1} kg^{-1}) at $T = 2.7$ K, with the largest adiabatic temperature change $T_{ad} = 23.2$ K for a field change of 8.9 T. At $T = 20$ K, the lattice entropy S_L is small enough compared to the magnetic entropy S_m, $S_m/S_L = 21.3$, which warrants its potential in 2 −20 K cryocoolers with both the Stirling and Carnot cycles. Though with relatively large exchange interactions, the layered A-type spin arrangement ultimately enhances the magnetocaloric coupling, raising the possibilities of designing magnetic refrigerants with a high ratio of cooling capacity to volume.

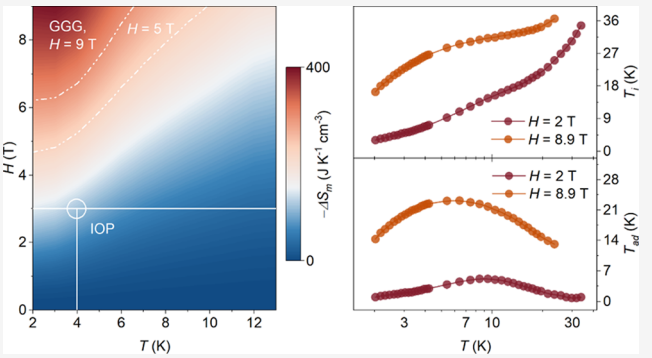

INTRODUCTION

Cooling by adiabatic demagnetization refrigerators (ADRs) relies on the magnetocaloric effect, which describes the entropy change associated with the temperature and the magnitude of applied fields.[1−4] Practical devices were first proposed by Giauque and Macdougall in 1933, by which cooling from 3.5 to 0.5 K was realized in a one-shot mode.[5] The constant low temperature was not maintained on ADRs until 1954, when successive cycles of magnetization were performed on a device constructed by Heer, Barnes, and Daunt.[6] Since then, research on magnetic cooling has expanded immensely, with expectations of more interesting possibilities in the matter below 20 K.

Though there is foreseeable complexity in the actualization of magnetic cooling, the high reliability, compactness, and efficiency with a few slow-moving parts warrant its potential for airborne and space refrigerators.[7,8] More recently, cyclic magnetic refrigerators were developed to liquefy H_2, He, or even to operate in the temperature range of the He^3−He^4 cryostat.[9−13] For these applications, a constant heat flow is required, thus working materials with a considerably high ratio of cooling capacity to mass or volume are desired.

If considering the thermodynamic parameters first, the working refrigerants should have a small lattice and electronic specific heat; otherwise, the internal heat load will increase.[8,14] In addition, any antiferromagnetic ordering should be avoided in the temperature range of interest. The available heat absorption capability lowers to nearly zero below the Néel ordering temperature, in which case it will be hardly accessible to self-cool the refrigerant.[15] Furthermore, a considerably large magnetic entropy change, $-\Delta S_m$, is necessary. This can be achieved by searching for working materials that possess large magnetic moments. The compounds containing gadolinium then become fairly appealing. There is virtually no orbital moment ($J = S = 7/2$) in Gd^{3+}, which has a spherically symmetric ground state of $^8S_{7/2}$ and an overall crystal field splitting of 1 K magnitude.[2,16−18] The gadolinium gallium garnet, $Gd_3Ga_5O_{12}$ (GGG), has long been used in varied prototype refrigerators with both single-crystal and polycrystalline forms.[7] $Gd(OH)_3$, $Gd(PO_3)_3$, $Gd_3Al_5O_{12}$, and many other paramagnetic materials were investigated in the test rig.[14]

Designing refrigerants with a high ratio of cooling capacity to volume requires high magnetic density, i.e., compacted magnetic ions and a relatively small fraction of non-magnetic elements, which inevitably bring complicated magnetic

Received: February 8, 2023
Published: March 21, 2023

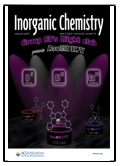

https://doi.org/10.1021/acs.inorgchem.3c00421
Inorg. Chem. 2023, 62, 5282−5291

interactions. Weaker exchange interactions between magnetic Gd^{3+} ions favor higher $-\Delta S_m$, as evidenced in frustrated perovskites A_2GdSbO_6 (A = Ca, Sr, Ba).[19] Thus, a compromise is necessary to control the magnetic density and the overall magnetocaloric coupling. Simply focusing on the available magnetic entropy changes is of course not enough, but maximizing the magnetic entropy density could reduce the field requirements, i.e., lower the cost. It should be noted that the overall performance cannot be optimized without considering the stability and processibility. Except for using single crystals, most of the device designs need porous refrigerant beds made from ceramic/composite powders, which will require the working materials to be chemically and physically rugged and also easy to fabricate.[7]

In our previous report, we have shown that the oxy-orthogermanate Gd_2GeO_5 exhibits a relatively large magnetic entropy change, $-\Delta S_m$ = 50.3 J K^{-1} kg^{-1} at 8.9 T.[20] It should be interesting to explore the magnetocaloric coupling in the structurally similar compound, oxyorthosilicate Gd_2SiO_5. First, research in scintillation crystals has revealed their high thermal stability, easy fabrication, and growth of both polycrystalline and single-crystal forms.[21,22] Also, structure analysis has shown that there is a large magnetic Gd^{3+} density with relatively light non-magnetic $[SiO_4]$ linkers, which may bring a low phonon contribution.[23] Furthermore, the layered stacking of $[GdO_x]$ polyhedra may bring interesting magnetic interactions. It should be noted that the expectations will be much higher while further considering the cost. The non-magnetic silicate is surely more economical than most metal elements.

Herein, we report the thermodynamic and magnetocaloric parameters of the X_1 phase polycrystalline Gd_2SiO_5. Low-temperature static magnetization and heat capacity measurements were performed. The magnetic correlations were analyzed by a mean-field approach as well as density functional theory (DFT) calculations. We show here that the layered magnetic configuration will ultimately enhance the magnetocaloric coupling. The figure of merits such as magnetic entropy change, adiabatic temperature change, relative cooling power, and lattice specific heat were quite impressive as compared to most of the magnetocaloric materials.

EXPERIMENTAL SECTION

Materials and Methods. Samples were prepared by flux-assisted solid-state synthesis: Gd_2O_3 (5N, Adamas, pre-dried at 1173 K overnight), silicon(IV) oxide (amorphous fumed, ~325 mesh, 3N, Alfa Aesar), and boric acid (4N, 3Achem) were ground to obtain fine powders. The flux ratio was set to be 3 wt % of the total amount of Gd_2O_3 and SiO_2. The so-obtained homogeneous mixture was pressed into pellets (φ − 1.8 cm, about 3 g weight) and calcined in a flow of air at 1373 K for 9 h, and then the pellets were pulverized and re-pelleted with a second heating to 1573 K for 18 h.

Characterizations. X-ray powder diffraction data were collected using monochromated Cu Kα radiation on a Huber diffraction and positioning equipment. The Rietveld refinements were performed using the GSAS package with the EXPGUI interface, of which the backgrounds were modeled by a Chebyshev polynomial of 10 terms.[24,25] The pseudo-Voigt function was used for modeling peak shapes.

Tablets of powders were used for magnetic measurements, which were compressed in a gold capsule of φ − 3 mm × 5 mm isostatically to a pressure of 5 GPa for 20 min. The dc susceptibility and magnetization isotherms were collected on a cryogen-free PPMS (PPMSDynaCool, Quantum Design). Calorimetry measurements were performed on a commercial physical property measurement system (PPMS-9, Quantum Design) in the temperature T of 1.9−40 K and in an external field of 0, 2, and 8.9 T using Apiezon N-grease to ensure thermal contact.

Simulation Methods and Models. Our DFT calculations were performed with the Vienna ab initio simulation package (VASP).[26,27] The generalized gradient approximation (GGA) proposed by Perdew, Burke, and Erzernhof was employed to describe the electronic exchange−correlation potentials.[28] A Hubbard U correction applied on the Gd 4f orbitals, U_f = 4.6 eV, was considered. The energy cutoff was set to be 550 eV, and the Brillouin zone was sampled with resolutions better than 0.02 $Å^{-1}$ under the scheme of Monkhorst-Pack.[29,30] Possibilities of spin polarization were allowed in all the calculations to explore long-range magnetic orderings. The ground state geometries were optimized until the total energies converged to 1×10^{-5} eV, and the Hellman-Feynman forces on each atom were less than 0.01 eV/Å.

We further considered the exchange coupling constants as introduced by Ruiz et al., where the antiferromagnetic coupling J_{AFM} was calculated using the following equation

$$J_{AFM} = \frac{E_{ls} - E_{hs}}{2S_iS_j} \tag{1}$$

in which the S_i and S_j are local spin values, E_{ls} represents the energy of a low-spin solution with antiferromagnetic couplings between the two paramagnetic centers, and E_{hs} corresponds to the energy of a high-spin (ferromagnetic) state, respectively.[31]

The real-space Hamiltonian of the ground state was interpolated with Wannier functions as implemented in the Wannier90 package.[32,33] The magnetic force theorem was used to compute the magnetic coupling energy between ions i and j

$$J_{ij} = \frac{1}{4\pi}\mathrm{Im}\int_{-\infty}^{E_f} \mathrm{d}E\mathrm{Tr}^{L}\{\Delta_i G_{ij}^{\uparrow}\Delta_j G_{ji}^{\downarrow}\} \tag{2}$$

in which E_f denotes the Fermi energy, $\Delta_{i(j)}$ is the exchange splitting in the shell of magnetic ions i and j, and $G^{\uparrow(\downarrow)}(E) = (E - H^{\uparrow(\downarrow)} + i\eta)^{-1}$ is Green's function of spin-up (spin-down) electrons. $H^{\uparrow(\downarrow)}$ is the real-space Hamiltonian of spin-up (spin-down) electrons, and η is set to 0.0001 eV. The Tr^L denotes the trace in orbitals.[34]

Theoretical Backgrounds. The isothermal magnetic entropy change can be related to the magnetization dependences by the thermodynamic Maxwell relation

$$\Delta S_m(H, T) = \int_0^H (\partial M/\partial T)_H \, \mathrm{d}H \tag{3}$$

of which the calculation is approximated by

$$\Delta S_m \approx \frac{1}{\Delta T}\left[\int_0^H M(T + \Delta T, H)\,\mathrm{d}H - \int_0^H M(T, H)\,\mathrm{d}H\right] \tag{4}$$

for magnetization data M collected at discrete temperature T and field H, ΔT represents temperature intervals.[35] Furthermore, the numerical calculation can be processed from the magnetic entropy data, by

$$\Delta S_m = S_m(T, H) - S_m(T, 0) \tag{5}$$

where $S_m(T,H)$ and $S_m(T,0)$ denote the magnetic entropy under the H and zero-field, the magnetic entropy is calculated by integration of the heat capacity C_p via $\int_0^T \frac{C_p}{T}\,\mathrm{d}T$.

The single Debye model was used to evaluate the lattice contributions (2 K < T < 40 K), as

$$C_L = \frac{9nN_Ak_BT^3}{\Theta_D^3}\int_0^{\Theta_D/T}\frac{x^4e^x}{(e^x-1)^2}\,\mathrm{d}x \tag{6}$$

where N_A and k_B are the Avogadro constant and Boltzmann constant, Θ_D denotes the Debye temperature, and n is the number of atoms per chemical formula, respectively.

https://doi.org/10.1021/acs.inorgchem.3c00421
Inorg. Chem. 2023, 62, 5282−5291

The heat capacity data processing starts from a paramagnetic model, where the magnetic entropy S_m is related to the partition function Z by

$$S_m/R = \mathrm{d}(T\ln Z)/\mathrm{d}T \quad (7)$$

In this case, the partition function has the form

$$Z = \sum_{I=-J}^{I=J} \exp \frac{IM_J H}{Jk_B T} \quad (8)$$

where $M_J = g\mu_B J$ represents the magnetic moment of one atom. Summation of eqs 7 and 8 gives the magnetic entropy S_m per mole as

$$S_m/R = \ln \sinh[(2J+1)x/2J]/\sinh(x/2J) - xB_J(x) \quad (9)$$

where $B_J(x)$ is the Brillouin function with $x = g\mu_B SH/k_B T$.

RESULTS AND DISCUSSION

X-ray Powder Diffraction Patterns. Figure 1a shows the Rietveld refinement of a powder X-ray diffraction pattern using the program GSAS with the EXPGUI interface.[25] All the observed reflections could be indexed into the $P2_1/c$ (14) space group, with systematic absences of $l \neq 2n$ and $k \neq 2n$ for $h0l$ and $0k0$ reflections. The derived structural parameters (calculated density ρ = 6.8 g cm^3) with a = 9.1288(6) Å, b = 7.0619(4) Å, c = 6.7431(4) Å, and β = 107.5685(9) ° are in accord with the previously reported X_1 phase Ln_2SiO_5 (Ln = Y and Gd).[23] The goodness of fit χ^2 is 3.868, with final reliability indices of wR_p/R_p = 0.0238/0.0175 = 1.36. The final positional and thermal parameters, and the selected interatomic distances (Å) and angles (°) are given in Tables S1−S3.

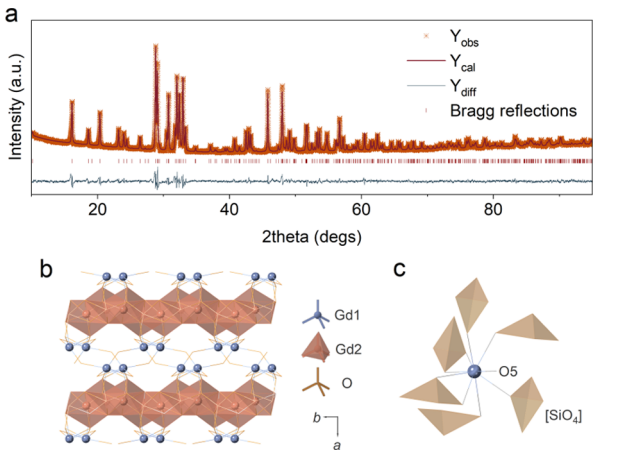

Figure 1. (a) Observed and calculated diffraction patterns for Gd_2SiO_5, along with the differences $Y_{obs} - Y_{cal}$ and the Bragg reflections (vertical bars). (b,c) Projection of the X_1 phase viewed along the c axis and the illustration of the [Gd1O$_9$] coordination.

There are two inequivalent Gd^{3+} sites in the three-dimensional X_1 phase structure, denoted as Gd1 and Gd2 sites. The first Gd1 site is bonded in a Gd1O$_9$ coordinate geometry with a spread of Gd1-O bond lengths ranging from 1.968(22) to 3.249(29) Å, forming a tricapped trigonal prism. The Gd2 site is coordinated in a sevenfold geometry, Gd2O$_7$, with a spread of Gd2−O bond lengths ranging from 2.120(17) to 2.696(23) Å, which can be described as a distorted hexagonal pyramid. The nine-coordinated Gd1O$_9$ can be viewed as infinite chains running along ⟨001⟩ in a face-sharing form, and the individual chains are further linked by oxygen faces. The sevenfold Gd2O$_7$ polyhedra share edges and form pucked two-dimensional (2D) networks parallel to the (100) plane, indicating possible competing magnetic interactions, as depicted in Figure 1b,c. These two kinds of polyhedra are alternately stacked in an AABAA pattern along a axis with an interlayer distance d_{12} = 3.741(3) Å, and are interlinked by [SiO$_4$] groups and the O5 oxygen atoms. The nearest neighbor nn distances of magnetic Gd^{3+} sites d_{nn} are 3.289(4) Å, which locate in the Gd1O$_9$ layer. The next and the third-next nearest neighbor distances, d_{nnn} and d_{tnn}, are in the 2D networks of Gd2O$_7$ polyhedra to be of 3.573(5) and 3.579(4) Å, respectively.

dc Susceptibility and Magnetization Measurements. The temperature-dependent magnetic susceptibility and its inverse form are shown in Figure 2a, with no anomaly indicative of any long-range magnetic ordering. A Curie−Weiss form with contributions of temperature-independent χ_0 is used to fit the inverse magnetic susceptibility, $\chi(T) = C/(T-\theta) + \chi_0$, which comprises contributions of closed-shell diamagnetic susceptibility and temperature-independent paramagnetic susceptibility. The best agreement of the fit accounting for the full temperature region is obtained by using $\chi_0 = 5.9 \times 10^{-4}$ emu mol^{-1} Oe^{-1} and correspondingly the Curie constant C = 7.5 emu mol^{-1} Oe^{-1} K and the Weiss temperature θ = −5.3 K, indicating predominant antiferromagnetic couplings.[36] The observed effective magnetic moment, $\mu_{obs} = (8C)^{1/2}$ = 7.75 μ_B, is in accordance with the theoretically isotropic ground state $^8S_{7/2}$ of Gd^{3+} ions (S = 7/2, L = 0, g = 2).

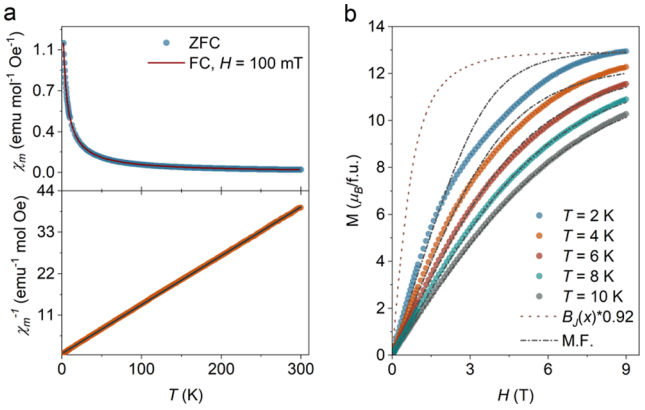

Figure 2. (a) Temperature dependences of magnetic susceptibilities (upper panel) and their inverse form (lower panel) measured under zero-field-cooled and field-cooled conditions. (b) Magnetization curves recorded at 2, 4, 6, 8, and 10 K. The dotted line shows a Brillouin function normalized to the experimental M(2 K, 9 T). The dash-dot line represents calculated magnetization performed by the mean-field (M.F.) method.

Figure 2b shows the raw magnetizations recorded at 2−10 K and their corresponding field-derivative curves, dM/dH, as a function of H (Figure S1). The curves exhibit monotonic and continuous behavior without clear signs of phase transition. No saturation moment is achieved even at the highest applicable field H = 9 T, which amounts to μ_{obs} = 12.9 μ_B/f.u., 92% of the theoretical moment of the non-interacted paramagnetic ions, i.e., the Brillouin function B_J(2 K, 9 T). Notably, the normalized $M(H)$ dependence of free magnetic ions with J = S = 7/2 saturates much more rapidly as compared to the experimental magnetizations, which show a linear trend up to ca. H = 2 T. Such a stark deviation usually indicates significant influences of antiferromagnetic interactions.[37]

https://doi.org/10.1021/acs.inorgchem.3c00421
Inorg. Chem. 2023, 62, 5282−5291

Analysis of Magnetic Couplings. In the case of isotropic exchange systems, a crude mean-field model can be used to probe the possible magnetic correlations.[7] This is performed by the assumption that the mean-field parameter, $\vec{H}_m$, is proportional to the degree of magnetic ordering. Thus, the total effective fields working on the spin sites in the Brillouin function read as $\vec{H}_{tot} = \vec{H}_{ext} + \vec{H}_m$, where $\vec{H}_{ext}$ denotes the external field. Here, we apply this model to evaluate the nearest neighbor exchange J_{nn} in Gd_2SiO_5, as in the target temperature range (T > 2 K) the system is nearly paramagnetic and therefore the quantum fluctuations are negligible.[19,20,37]

Since the orbital momentum L = 0 in Gd^{3+} ions, the mean exchange field, $\vec{H}_m$, can be converted to the exchange constant J_{nn} by translating the exchange Hamiltonian, which gives

$$\vec{H}_m = \frac{J_{nn} N_{ave}}{g^2 \mu_B} M\vec{n} \tag{10}$$

with N_{ave} representing the number of nearest neighbors, and M, $\vec{n}$ corresponding to the bulk magnetization in units of the Bohr magneton μ_B and the unit vector in the orientation of the external field, g is the Lande factor.[37] The field and temperature dependence of the bulk magnetization is then given by finding the roots of the transcendental function with a non-linear least squares method

$$f(M) = M - gSB_J(|\vec{H}_{ext} + \vec{H}_m|, T) \tag{11}$$

The free spin magnetization, $M = gSB_J(|\vec{H}_{ext}|, 6K)$, was used as the initial guess of the iteration, with a scale factor of M(9 T, 6 K)/M_{exp}(9 T, 6 K), the experimental value of the magnetization at field H = 9 T and temperature T = 6 K.

The resulting modeled curves with the optimized nn exchange parameter, J_{nn} = 0.28 K, produce the field dependences fairly well, especially at T > 4 K (dash dot lines in Figure 2b). If the number of nn was set to 4, a standard mean-field estimate of the Weiss temperature, $|\theta| = N_{ave}J_{nn}S(S + 1)/3 \approx 5.9$ K, was obtained, accurately captured the value determined from the static susceptibility measurements. However, the overall fitting suffers from an inconsistency in the field range of 2.5 < H < 7 T for isothermal magnetization at T = 2 and 4 K, which may arise from short-range correlations or field-induced spin rotations. Further neutron magnetic diffuse scattering experiments are needed to probe this deviation. If considering the dipolar interaction, D, defined as $D = D_{nn}/(S^2+S)$, of which the $D_{nn} = \mu_0\mu_{eff}^2/4\pi k_B R_{nn}^3$ nn, a D = 0.056 K is obtained with the nn set to 4. The small dipolar interaction D is helpful for the magnetocaloric performance, as declared by Koskelo et al.[19]

DFT Simulation. The magnetic and electronic structures were investigated using DFT within the GGA.[28] A Hubbard U = 4.6 eV was applied to the Gd^{3+} 4f orbitals. Magnetic ordering was explored by calculating the energies of conventional unrestricted collinear spin arrangements, of which supercells containing eight Gd^{3+} ions (four at the Gd1 site and the other four at the Gd2 site) with magnetic moments parallel to the z axis (z^+ and z^-) were constructed. The ground state structure was determined by searching for the most energetically favorable configurations among all the C(8,4) antiferromagnetic and the one ferromagnetic model. An A-type ground state was identified, where antiferromagnetic correlations exerted between the ferromagnetically coupled layers of Gd^{3+}, as depicted in Figure 3. The energy difference between the ferromagnetic configuration (E_{FM}) and the A-type antiferromagnetic correlations (E_{AFM}), $\Delta_E = E_{FM} - E_{AFM}$ = 16 meV/f.u. The calculated magnetic moments of Gd^{3+} for z^+ and z^- are 7.011 and 7.017 μ_B, in broad agreement with the spin-only value.

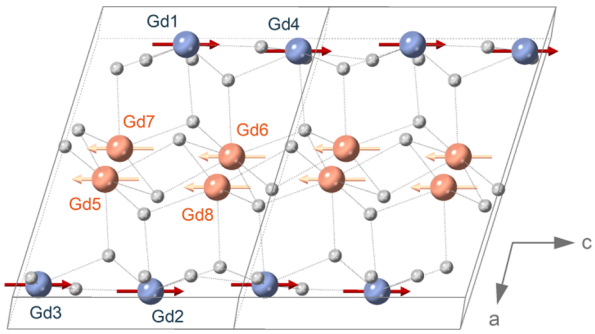

Figure 3. Computational unit cells with the lowest energy, atoms of Gd and O are depicted in balls, and the collinear spin arrangements are shown as arrows.

We then calculated the exchange coupling constants of 20 Gd^{3+} ion pairs using the magnetic force theorem.[34] The strongest exchange interactions, denoted as J_1, lie in the ferromagnetic layers formed by $Gd1O_9$ polyhedra. The ferromagnetic interactions in the Gd_2O_7 layer are also fairly strong, as listed in Table S4. These competitive interactions will suppress or at least lower the long-range antiferromagnetic ordering temperature, making Gd_2SiO_5 suitable for cooling at 2 to 20 K. Furthermore, the overall layered configuration favors magnetic decoupling of Gd^{3+} ions along the crystallographic axis, i.e., a much easier spin rotation process, thus ultimately enhancing the magnetocaloric effect, as in the α-$NaFeO_2$ type $NaGdS_2$ with two-dimensional $[GdS_2]^-$ layers.[38]

The average exchange interactions J_{ex} on the basis of the classical Heisenberg model in the framework of DFT total energies was also calculated.[31,39] The low-spin state is defined as the A-type structure of a fully optimized spin configuration, while the internal coordinates are kept static for calculations of the high-spin state. The relative total energies mapped onto the Hamiltonian can be then calculated by eq 1, giving a J_{ex} = 0.30 K. Interestingly, the DFT-derived magnetic exchange interaction agrees well with the mean-field estimate, further supporting the validity of our aforementioned magnetic coupling analysis.

The calculated band structures are shown in Figure 4a,c, which confirms that the X_1 phase Gd_2SiO_5 is insulating with a 4.85 eV gap. Insulating materials are better magnetocaloric candidates for their lowered eddy current in low temperatures.[7] Figure 4b shows the partial density of states of two Gd^{3+} ions with magnetic moments parallel (z^+) and antiparallel (z^-) to the z axis. The 4f states are highly localized and responsible for the gapped electronic structure, where the spin-up f of Gd^{3+} (z^+) is distributed between −3.5 and −5.0 eV. Meanwhile, in Gd^{3+} (z^-) the spin-up channels are in the range of 5.0 and 7.0 eV. The main hybridization of Gd^{3+} and O^{2-} comes from the 4f−2p orbitals, as depicted in Figure 4b.

Specific Heat and Magnetic Entropy. Figure 5a shows the heat capacity, C_p, measured at magnetic fields of H = 0, 2, and 8.9 T. The results are plotted on a semilog scale. No magnetic ordering is observed in the zero-field measurements, but a $\propto T^{-2}$ dependence in the low-temperature region indicates antiferromagnetic transitions.[40] The single Debye

https://doi.org/10.1021/acs.inorgchem.3c00421
Inorg. Chem. 2023, 62, 5282−5291

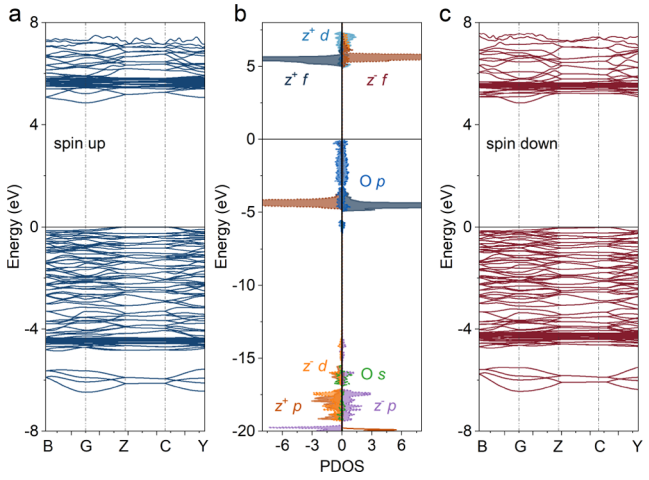

Figure 4. Spin polarized band structures of up (a) and down states (c), and the density of states for two Gd^{3+} ions with positive and negative spin alignments (b).

model cannot produce the lattice contributions very well below 40 K, while the polynomial $BT^3 + CT^5 + DT^7$ describes the term nicely. Fitting of the high-temperature zero-field data gives a lattice specific heat constant, $\alpha = 5.3 \times 10^{-5}$, comparable to the well-known refrigerant material $Gd_3Ga_5O_{12}$ (GGG, $\alpha = 3 \pm 0.3 \times 10^{-5}$).[7]

The entropy can be then computed as $S = \int_{T_1}^{T_2} C_p \, dT/T$, in which the absolute values are usually made by taking $T_1 = 0$. This process is reasonable for high fields; in our case $H = 8.9$ T, where the C_p data can be properly extrapolated. However, the blind extrapolation fails for fields of 0 and 2 T. The *s*-state Gd^{3+} shows negligible crystal-field splits (<1 K), which means the integration of C_p/T through the antiferromagnetic region should result in the full entropy *R*ln8 per mole Gd^{3+} ion.[40] There are no measurements below 2 K, so here we have adopted a mean-field estimate, as illustrated in 7.[7,41−43]

In a simple antiferromagnetic system, and for $T > T_N$, the expression H/T can be replaced by a mean-field approximation, $H/(T + T_{M.F.})$.[43] Then eq 9 with an adjusted $T_{M.F.}$ was used to fit the high temperature data for $H = 8.9$ T, giving an optimized $T_{M.F.} = 0.5$ K. The discrepancies between the estimated and measured entropies at 2 and 8.9 T are used to modify the $S-T$ diagrams, while for zero-field data, full magnetic entropy *R*ln8 is used (Figure 5b). Lattice entropies are calculated as $S_L = 1/3BT^3 + 1/5CT^5 + 1/7DT^7$. The consolidation process is not very precise but can indeed bring the entropy results into closer agreement with experimental values.

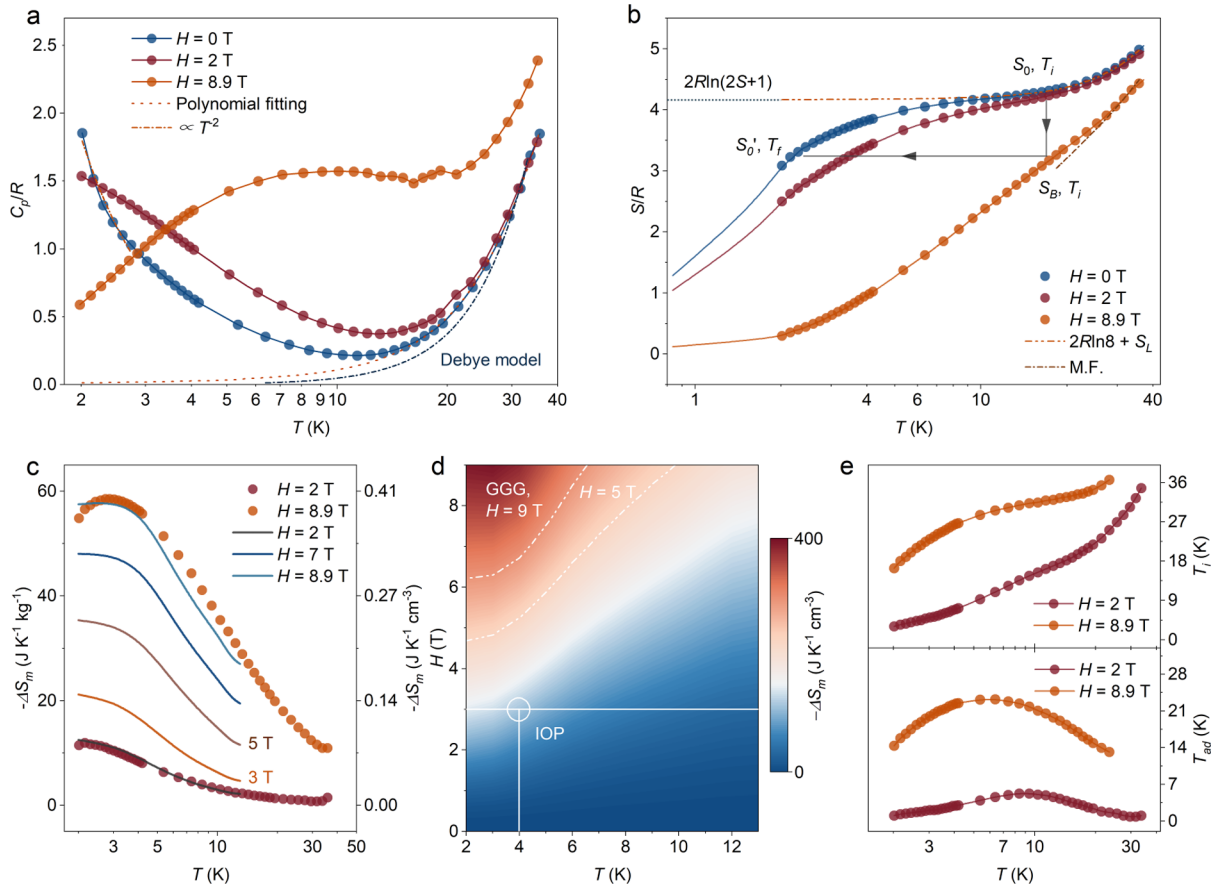

Figure 5. (a) Heat capacity of Gd_2SiO_5 at various magnetic fields, normalized to *R*, in a semilog scale. The Debye model and polynomial fitting data are plotted as dotted lines. (b) Calculated and measured entropies of Gd_2SiO_5 at various magnetic fields of $H = 0$, 2, and 8.9 T. The calculation uses the mean-field approximation as discussed in the text. Arrows show the adiabatic demagnetization and magnetization processes. (c) Magnetocaloric effect of Gd_2SiO_5 as obtained from heat capacity (close marks) and the isothermal magnetization data (solid lines), under magnetic field changes of 2, 3, 5, 7, and 8.9 T. (d) Contour plots showing the figure of merit for the magnetocaloric effect, the dotted white lines denote $-\Delta S_m$ of GGG. (e) Adiabatic temperature increments (upper panel) and changes (down panel) from zero field to the indicated applied fields.

https://doi.org/10.1021/acs.inorgchem.3c00421
Inorg. Chem. 2023, 62, 5282−5291

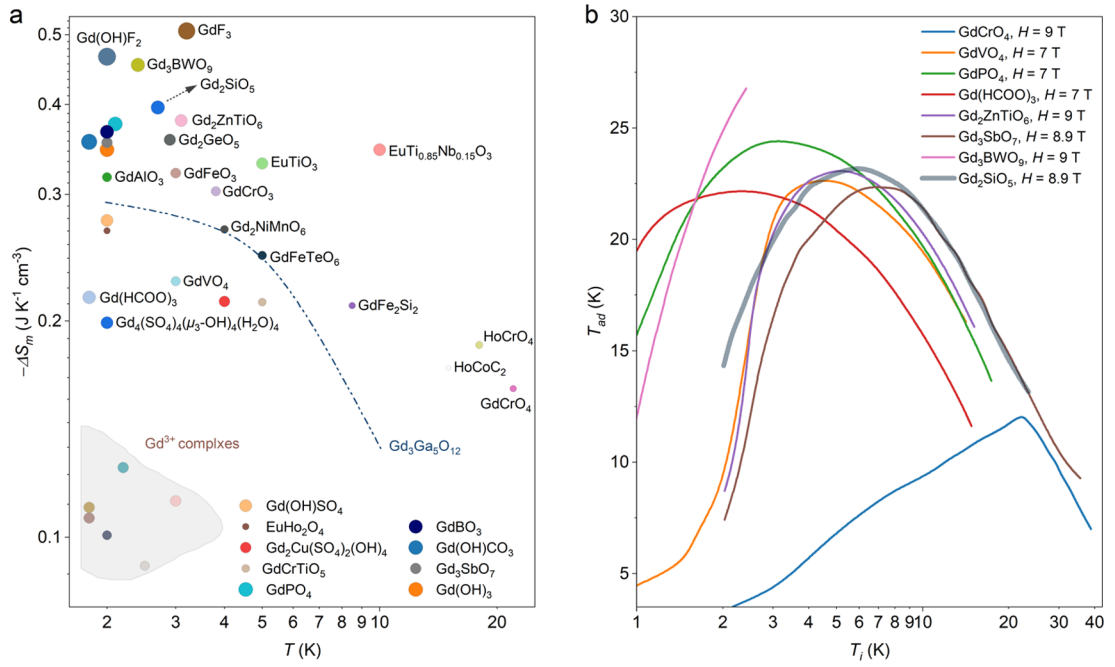

Figure 6. (a) Magnetic entropy change $-\Delta S_m$ for some representative magnetocaloric materials under field change of $H \geq 7$ T, bubble area represents $-\Delta S_m$ values in gravimetric units (detailed information is listed in Table S5). The dotted line corresponds to the performances of GGG. (b) Comparisons of T_{ad} with several top-performing magnetocaloric materials.[41−43,47−69] Reproduced with permission from ref 41. Copyright 2022 Springer Nature. Reproduced with permission from ref 42. Copyright 2014 American Physical Society. Reproduced with permission from ref 43. Copyright 2018 American Physical Society. Reproduced with permission from ref 47. Copyright 2013 John Wiley & Sons, Inc. Reproduced with permission from ref 48. Copyright 2020 The Royal Society of Chemistry. Reproduced with permission from ref 50. Copyright 2016 American Physical Society. Reproduced with permission from ref 68. Copyright 2021 The Royal Society of Chemistry.

Magnetocaloric Effect. The validity of our data consolidation can also be verified by the magnetic entropy change results. Using the well-known Maxwell relation, the isothermal magnetic entropy increments are numerically approximated by eq 4.[35] Data processing from the heat capacity data, eq 5, illustrated as point (S_0, T_i) to point (S_B, T_i) is also plotted (Figure 5b). The two computing results overlap quite well, as shown in Figure 5c.

Under an external field change of H = 8.9 T, the magnetic entropy change $-\Delta S_m$ is 58.5 J K^{-1} kg^{-1} at 2.7 K and 0.40 J K^{-1} cm^{-3} in volumetric units. This value is fairly large when compared to the benchmark magnetic refrigerant GGG (42.4 J K^{-1} kg^{-1} and 0.3 J K^{-1} cm^{-3} at 9 T), as shown in the contour plot (Figure 5d).[7,44] If considering the low-field helium liquefaction, a value of 0.11 J K^{-1} cm^{-3} is reserved, marked as the interesting operation point at 4 K and 3 T, also validating its potential use in low-field ADR cryostat stages.[20,45]

The magnetic entropy change of Gd_2SiO_5 outperforms most of the magnetocaloric compounds with dense Gd^{3+} spins, as was shown in the bubble chart (Figure 6a) and Table S5. Furthermore, the Gd_2SiO_5 also prevails in another figure of merit, the relative cooling power RCP, which is defined as the product of the maximum entropy change and the corresponding full width at half-maximum of the $-\Delta S_m$ curve, RCP = $-\Delta S_{max}\delta T_{fwhm}$, to be of 649.5 J kg^{-1} (4.4 J cm^{-3}).[46] The value of $-\Delta S_m$ in the unit of per mole Gd^{3+} ions is 71.5% of that of the theoretical value 2Rln8, at a field change of H = 8.9 T, which is lower than some magnetocaloric materials with weaker super-exchange interactions, such as the Ca_2GdSbO_6 and $Gd(HCOO)_3$.[19,47] Further work on making ultrafine particles of Gd_2SiO_5 shall be interesting, which will enhance the magnetocaloric effect due to disturbed long-range interactions. Though with a considerably large super-exchange interaction, J_{ex} = 0.28 K, the small dipolar interaction, D = 0.056 K, as well as the ferromagnetic Gd^{3+} layers, make the decoupling easier. The layered A-type magnetic configuration ultimately enhances the magnetocaloric coupling as compared to Gd_2GeO_5 ($-\Delta S_m$ = 0.36 J K^{-1} cm^{-3} at 8.9 T), which is crystallographically similar to Gd_2SiO_5 but with a different antiferromagnetic ground state.[20] Besides, the A-type antiferromagnetic Gd_3BWO_9 with a volumetric performance of $-\Delta S_m$ = 0.45 J K^{-1} cm^{-3} at 9 T also verifies the abovementioned conclusions.[48]

Figure 5e shows the theoretical temperature changes associated with changes in the applied field. The estimating method is depicted in Figure 5b. Taking the best point (S_B, T_i) to (S_0', T_f), for instance, if the Gd_2SiO_5 is at T_i = 29.6 K in a magnetic field of H = 8.9 T, reducing the field to H = 0 results in a temperature fall to T_f = 6.4 K, denoted as T_{ad} = 23.2 K. It should be noted that the interpretation of temperature increments is more complicated in practical cases as the above-described processes cannot be truly adiabatic. The demagnetized target field is generally larger than zero so as to stabilize the heat leaks.[7] Notably, the adiabatic temperature change T_{ad} is impressive when compared to the GGG (20.0 K under a field change of 9.4 → 0.7 T) and compares favorably to a list of top-performing magnetocaloric materials, as depicted in Figure 6b.

Table 1 shows a list of several choices for 2 to 20 K refrigerators. The working materials should have a small molar volume V_{mol} and a low magnetic ordering temperature (T_{order} below the lowest working window), for which criteria the Gd_2SiO_5 performs very well.[8] Furthermore, the lattice entropy

https://doi.org/10.1021/acs.inorgchem.3c00421
Inorg. Chem. 2023, 62, 5282−5291

Table 1. Comparison of Thermodynamic Parameters for Several Magnetocaloric Compounds

formula	V_{mol}/cm^3	T_{order}/K	α/K^{-3}	S_m/S_L	refs
Gd_3BWO_9	34.6	1.0	6.8×10^{-5}	10.2	48
Gd_2ZnTiO_6	35.2	2.43	6.1×10^{-5}	24.4	68
$GdPO_4$	49.5	0.8	6×10^{-5}[a]	2.4	14
$Gd(OH)_3$	37	2–4.1	1.8×10^{-6}	9.6	14
$Gd_2(SO_4)_3{\cdot}8H_2O$	120	0.18	2×10^{-4}	1.1	14
Gd_3SbO_7	30.3	2.4	1.1×10^{-4}	15.6	41
Gd_2SiO_5	31.2	1.5[b]	5.3×10^{-5}	21.3	this work

[a]Taken from the value of $DyPO_4$. [b]Estimated via the method in ref 7.

S_L at 20 K contributes a relatively low fraction of the magnetic entropy S_m, $S_m/S_L = 21.3$, making Gd_2SiO_5 applicable for both the Stirling and the Carnot cycles.

Power Law Analysis. The field dependences of the relative cooling power, RCP, and the maximum magnetic entropy change, $-\Delta S_{max}$, were examined following the scaling relations $RCP \propto H^{1+\delta}$ and $-\Delta S_m \propto H^n$, respectively.[70,71] A $\delta = 1.5$ and $n = 1.1$ were produced (Figure 7a). By further expanding the power law to the general field dependence of the magnetic entropy change, $-\Delta S_m \propto H^n$, we obtained an exponent that was locally calculated in the expression

$$n(H, T) = \frac{d \ln|\Delta S_m|}{d \ln H} \tag{12}$$

as was depicted in Figure 7b.[72,73] We found a trend of $n(H,T)$ in the isothermal curves (2–13 K) to the paramagnetic value 2, indicating a second-order phase transition. The regions of low applied fields (<0.1 T) are omitted, as under these small fields the samples are possibly in a "multi-domain" state.[73]

We then adopt a qualitative criterion to identify the thermomagnetic phase transitions, as devised by Franco et al.[71,74,75] The procedure is based on rescaled curve construction, assuming that the equivalent points of the different $-\Delta S_m$ curves overlap each other. By normalizing the $-\Delta S_m$ curves with respect to their maximum values, $-\Delta S_{max}$, and rescaling the temperature axis to a reduced form, T_{red}, the phenomenological universal curves can be constructed. Here, the T_{red} is defined as $T_{red} = (T - T_{max})/(T_{ref} - T_{max})$, in which the T_{ref} is experiencedly determined to be the temperature corresponding to $\Delta S_m(T_{ref}) = 1/2\Delta S_{max}$. A total of 109 curves of different applied fields are processed, which forms a fairly nice single master curve and resembles those magnetocaloric systems with a second-order phase transition, as depicted in Figure 7c.

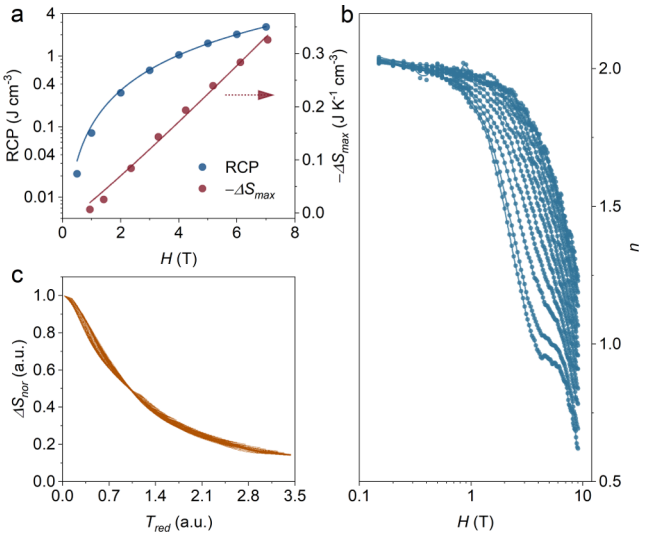

Figure 7. (a) Power law analysis of the field variance of peak magnetic entropy change $-\Delta S_{max}$, and the relative cooling power RCP. (b) Temperature and field variance of the exponent $n(H,T)$ in isothermal curves (2–13 K). (c) Phenomenological universal curves derived from a total of 109 applied fields.

CONCLUSIONS

Our survey of the magnetocaloric parameters shows that the X_1 phase Gd_2SiO_5 would be a strong candidate for cryogenic magnetic coolers. An antiferromagnetic exchange parameter, $J_{nn} = 0.28$ K, is determined from the mean-field analysis of the static $M(H)$ dependences, in accordance with the DFT calculations. Though with relatively strong exchange interactions, the magnetocaloric effect of Gd_2SiO_5 is quite large and superior to most of the rare earth compounds reported to date, especially in terms of magnetic entropy change (0.40 J K^{-1} cm^{-3} at 8.9 T), adiabatic temperature change (23.2 K at 8.9 T), relative cooling power (4.4 J cm^{-3} at 8.9 T), and lattice heat capacity ($\alpha = 5.3 \times 10^{-5}$). Considering the thermodynamic parameters, the lattice entropy S_L is small enough compared to the magnetic entropy S_m at $T = 20$ K, $S_m/S_L = 21.3$, which warrants its potential in 2 to 20 K cryocoolers with both the Stirling and Carnot cycles. The work here should shed a light on designing magnetic refrigerants with a high volumetric performance at varied temperatures, i.e., exploring systems with a layered magnetic structure, especially those with an A-type magnetic configuration. Besides, further work concerning chemical tunability will be interesting, such as the replacement of $[SiO_4]$ to $[MoO_4]/[WO_4]$ linkers or the non-equivalent substitution of Si^{4+} to $Mn^{3+}/Fe^{3+}/Co^{3+}$ to make magnetic clusters.

ASSOCIATED CONTENT

Supporting Information

The Supporting Information is available free of charge at https://pubs.acs.org/doi/10.1021/acs.inorgchem.3c00421.

Field-derivative magnetization curves, crystallographic data, magnetic coupling constants, and some representative magnetocaloric materials (PDF)

AUTHOR INFORMATION

Corresponding Authors

Hongzhi Cui − *College of Civil and Transportation Engineering, College of Physics and Optoelectronic Engineering, Shenzhen University, Shenzhen 518060, China*; Email: h.z.cui@szu.edu.cn

Yu-Jia Zeng − *College of Civil and Transportation Engineering, College of Physics and Optoelectronic Engineering, Shenzhen University, Shenzhen 518060, China*; orcid.org/0000-0001-5673-3447; Email: yjzeng@szu.edu.cn

Youwen Long − *Beijing National Laboratory for Condensed Matter Physics, Institute of Physics, Chinese Academy of Sciences, Beijing 100190, China; School of Physical Sciences, University of Chinese Academy of Sciences, Beijing 100049, China; Songshan Lake Materials Laboratory, Dongguan*

https://doi.org/10.1021/acs.inorgchem.3c00421
Inorg. Chem. 2023, 62, 5282−5291

523808 Guangdong, China; orcid.org/0000-0002-8587-7818; Email: ywlong@iphy.ac.cn

Authors

Ziyu W. Yang − *College of Civil and Transportation Engineering, College of Physics and Optoelectronic Engineering, Shenzhen University, Shenzhen 518060, China; Beijing National Laboratory for Condensed Matter Physics, Institute of Physics, Chinese Academy of Sciences, Beijing 100190, China;* orcid.org/0000-0003-3139-2767

Jie Zhang − *Beijing National Laboratory for Condensed Matter Physics, Institute of Physics, Chinese Academy of Sciences, Beijing 100190, China; School of Physical Sciences, University of Chinese Academy of Sciences, Beijing 100049, China*

Dabiao Lu − *Beijing National Laboratory for Condensed Matter Physics, Institute of Physics, Chinese Academy of Sciences, Beijing 100190, China; School of Physical Sciences, University of Chinese Academy of Sciences, Beijing 100049, China*

Xiaoxiao Zhang − *Beijing National Laboratory for Condensed Matter Physics, Institute of Physics, Chinese Academy of Sciences, Beijing 100190, China; School of Physical Sciences, University of Chinese Academy of Sciences, Beijing 100049, China*

Haoting Zhao − *Beijing National Laboratory for Condensed Matter Physics, Institute of Physics, Chinese Academy of Sciences, Beijing 100190, China*

Complete contact information is available at: https://pubs.acs.org/10.1021/acs.inorgchem.3c00421

Author Contributions

Z.Y.: conceptualization, investigation, formal analysis, writing—original draft, and funding acquisition. J.Z., D.L., X.Z., and H.Z.: investigation. H.C., Y.J.Z., and Y.L.: supervision and funding acquisition.

Notes

The authors declare no competing financial interest.

■ ACKNOWLEDGMENTS

This work was performed through support of the National Key R&D Program of China [grant numbers 2021YFA1400300 and 2018YFA0305700]; the Guangdong Basic and Applied Basic Research Foundation [grant number 2022A1515111009]; the Science, Technology, and Innovation Commission of Shenzhen Municipality [grant numbers JCYJ20190808152217447 and JCYJ20210324095611032]; the National Natural Science Foundation of China [grant numbers 51925804, 11934017, 11921004, and 52273298]; the Beijing Natural Science Foundation [grant number Z200007]; and the Chinese Academy of Sciences [grant number XDB33000000].

■ REFERENCES

(1) Barclay, J. A. Magnetic refrigeration: a review of a developing technology. *Adv. Cryog. Eng.* **1988**, *33*, 719.

(2) Franco, V.; Blázquez, J. S.; Ipus, J. J.; Law, J. Y.; Moreno-Ramírez, L. M.; Conde, A. Magnetocaloric effect: From materials research to refrigeration devices. *Prog. Mater. Sci.* **2018**, *93*, 112.

(3) Lai, J.; Bolyachkin, A.; Terada, N.; Dieb, S.; Tang, X.; Ohkubo, T.; Sepehri-Amin, H.; Hono, K. Machine learning assisted development of Fe2P-type magnetocaloric compounds for cryogenic applications. *Acta Mater.* **2022**, *232*, 117942.

(4) Hardy, V.; Hamane, R.; Veillon, F.; Risser, M.; Guillou, F. "Two-steps" process in the first-order transformation of giant magnetocaloric materials. *Acta Mater.* **2022**, *231*, 117869.

(5) Giauque, W. F.; MacDougall, D. P. Attainment of Temperatures Below 1° Absolute by Demagnetization of $Gd_2(SO_4)_3{\cdot}8H_2O$. *Phys. Rev.* **1933**, *43*, 768.

(6) Heer, C. V.; Barnes, C. B.; Daunt, J. G. The Design and Operation of a Magnetic Refrigerator for Maintaining Temperatures below 1 K. *Rev. Sci. Instrum.* **1954**, *25*, 1088.

(7) Barclay, J. A.; Steyert, W. A. Materials for magnetic refrigeration between 2 K and 20 K. *Cryogenics* **1982**, *22*, 73.

(8) Barclay, J. A.; Steyert, W. A. *Magnetic Refrigeration for Space Applications: Report on a Design Study*; Los Alamos National Laboratory (LANL): Los Alamos, NM (United States), 1980.

(9) Numazawa, T.; Hashimoto, T.; Nakagome, H.; Tanji, N.; Horigami, O. *Advances in Cryogenic Engineering*; Fast, R. W., Ed.; Springer US: Boston, MA, 1984; Vol. *29*.

(10) Nakagome, H.; Kuriyama, T.; Ogiwara, H.; Fujita, T.; Yazawa, T.; Hashimoto, T. *Advances in Cryogenic Engineering*; Fast, R. W., Ed.; Springer US: Boston, MA, 1986; Vol. *31*.

(11) Jahromi, A. E.; Miller, F. K. Development of a He3−He4 sub Kelvin active magnetic regenerative refrigerator (AMRR) with no moving parts. *AIP Conf. Proc.* **2014**, *1573*, 253.

(12) Numazawa, T.; Kamiya, K.; Utaki, T.; Matsumoto, K. Magnetic refrigerator for hydrogen liquefaction. *Cryogenics* **2014**, *62*, 185.

(13) Castro, P. B. d.; Terashima, K.; Yamamoto, T. D.; Hou, Z.; Iwasaki, S.; Matsumoto, R.; Adachi, S.; Saito, Y.; Song, P.; Takeya, H.; Takano, Y. Machine-learning-guided discovery of the gigantic magnetocaloric effect in HoB2 near the hydrogen liquefaction temperature. *NPG Asia Mater.* **2020**, *12*, 35.

(14) Pratt, W. P., Jr.; Rosenblum, S. S.; Steyert, W. A.; Barclay, J. A. A continuous demagnetization refrigerator operating near 2 K and a study of magnetic refrigerants. *Cryogenics* **1977**, *17*, 689−693.

(15) Wikus, P.; Burghart, G.; Figueroa-Feliciano, E. Optimum operating regimes of common paramagnetic refrigerants. *Cryogenics* **2011**, *51*, 555.

(16) Balli, M.; Jandl, S.; Fournier, P.; Kedous-Lebouc, A. Advanced materials for magnetic cooling: Fundamentals and practical aspects. *Appl. Phys. Rev.* **2017**, *4*, 021305.

(17) Lyubina, J. Magnetocaloric materials for energy efficient cooling. *J. Phys. D: Appl. Phys.* **2017**, *50*, 053002.

(18) Newman, D. J. The ground state splitting in Gd^{3+} and Eu^{2+}. *Solid State Commun.* **1976**, *18*, 667.

(19) Koskelo, E. C.; Liu, C.; Mukherjee, P.; Kelly, N. D.; Dutton, S. E. Free-Spin Dominated Magnetocaloric Effect in Dense Gd^{3+} Double Perovskites. *Chem. Mater.* **2022**, *34*, 3440.

(20) Yang, Z. W.; Qin, S.; Zhang, J.; Lu, D.; Zhao, H.; Kang, C.; Cui, H.; Long, Y.; Zeng, Y.-J. Gadolinium oxyorthogermanate Gd_2GeO_5: An efficient solid refrigerant material for magnetic cryocoolers. *Mater. Today Phys.* **2022**, *27*, 100810.

(21) Brandle, C. D.; Valentino, A. J.; Berkstresser, G. W. Czochralski growth of rare-earth orthosilicates Ln_2SiO_5. *J. Cryst. Growth* **1986**, *79*, 308−315.

(22) Cooke, D. W.; McClellan, K. J.; Bennett, B. L.; Roper, J. M.; Whittaker, M. T.; Muenchausen, R. E.; Sze, R. C. Crystal growth and optical characterization of cerium-doped $Lu_{1.8}Y_{0.2}SiO_5$. *J. Appl. Phys.* **2000**, *88*, 7360.

(23) Fukuda, K.; Iwata, T.; Champion, E. Crystal structure of lanthanum oxyorthosilicate, La_2SiO_5. *Powder Diffr.* **2006**, *21*, 300.

(24) Rietveld, H. A profile refinement method for nuclear and magnetic structures. *J. Appl. Crystallogr.* **1969**, *2*, 65.

(25) Toby, B. EXPGUI, a graphical user interface forGSAS. *J. Appl. Crystallogr.* **2001**, *34*, 210.

(26) Kresse, G.; Hafner, J. Ab initiomolecular dynamics for liquid metals. *Phys. Rev. B: Condens. Matter Mater. Phys.* **1993**, *47*, 558.

(27) Kresse, G.; Furthmüller, J. Efficient iterative schemes forab initiototal-energy calculations using a plane-wave basis set. *Phys. Rev. B: Condens. Matter Mater. Phys.* **1996**, *54*, 11169.

(28) Perdew, J. P.; Burke, K.; Ernzerhof, M. Generalized Gradient Approximation Made Simple. *Phys. Rev. Lett.* **1996**, *77*, 3865.
(29) Dudarev, S. L.; Botton, G. A.; Savrasov, S. Y.; Humphreys, C. J.; Sutton, A. P. Electron-energy-loss spectra and the structural stability of nickel oxide: An LSDA+U study. *Phys. Rev. B: Condens. Matter Mater. Phys.* **1998**, *57*, 1505.
(30) Monkhorst, H. J.; Pack, J. D. Special points for Brillouin-zone integrations. *Phys. Rev. B: Solid State* **1976**, *13*, 5188.
(31) Cremades, E.; Gómez-Coca, S.; Aravena, D.; Alvarez, S.; Ruiz, E. Theoretical Study of Exchange Coupling in 3d-Gd Complexes: Large Magnetocaloric Effect Systems. *J. Am. Chem. Soc.* **2012**, *134*, 10532.
(32) Pizzi, G.; Vitale, V.; Arita, R.; Blügel, S.; Freimuth, F.; Géranton, G.; Gibertini, M.; Gresch, D.; Johnson, C.; Koretsune, T.; Ibañez-Azpiroz, J.; Lee, H.; Lihm, J. M.; Marchand, D.; Marrazzo, A.; Mokrousov, Y.; Mustafa, J. I.; Nohara, Y.; Nomura, Y.; Paulatto, L.; Poncé, S.; Ponweiser, T.; Qiao, J.; Thöle, F.; Tsirkin, S. S.; Wierzbowska, M.; Marzari, N.; Vanderbilt, D.; Souza, I.; Mostofi, A. A.; Yates, J. R. Wannier90 as a community code: new features and applications. *J. Phys.: Condens. Matter* **2020**, *32*, 165902.
(33) Mostofi, A. A.; Yates, J. R.; Pizzi, G.; Lee, Y.-S.; Souza, I.; Vanderbilt, D.; Marzari, N. An updated version of wannier90: A tool for obtaining maximally-localised Wannier functions. *Comput. Phys. Commun.* **2014**, *185*, 2309.
(34) Liechtenstein, A. I.; Katsnelson, M.; Antropov, V.; Gubanov, V. Local spin density functional approach to the theory of exchange interactions in ferromagnetic metals and alloys. *J. Magn. Magn. Mater.* **1987**, *67*, 65.
(35) McMichael, R. D.; Ritter, J. J.; Shull, R. D. Enhanced magnetocaloric effect in $Gd_3Ga_{5-x}Fe_xO_{12}$. *J. Appl. Phys.* **1993**, *73*, 6946.
(36) Yang, Z.; Zhang, H.; Xu, J.; Ma, R.; Sasaki, T.; Zeng, Y. J.; Ruan, S.; Hou, Y. Anisotropic fluoride nanocrystals modulated by facet-specific passivation and their disordered surfaces. *Natl. Sci. Rev.* **2020**, *7*, 841.
(37) Wellm, C.; Zeisner, J.; Alfonsov, A.; Sturza, M. I.; Bastien, G.; Gaß, S.; Wurmehl, S.; Wolter, A. U. B.; Büchner, B.; Kataev, V. Magnetic interactions in the tripod kagome antiferromagnet $Mg_2Gd_3Sb_3O_{14}$ probed by static magnetometry and high-field ESR spectroscopy. *Phys. Rev. B* **2020**, *102*, 214414.
(38) Delacotte, C.; Pomelova, T. A.; Stephant, T.; Guizouarn, T.; Cordier, S.; Naumov, N. G.; Lemoine, P. $NaGdS_2$: A Promising Sulfide for Cryogenic Magnetic Cooling. *Chem. Mater.* **2022**, *34*, 1829.
(39) Ruiz, E.; Alvarez, S.; Cano, J.; Polo, V. About the calculation of exchange coupling constants using density-functional theory: The role of the self-interaction error. *J. Chem. Phys.* **2005**, *123*, 164110.
(40) Hill, R. W.; Cosier, J.; Hukin, D. A. The specific heats of LaAg, GdAg and Gd_2O_3 from 0.5 to 22 K. *J. Phys. C: Solid State Phys.* **1983**, *16*, 2871.
(41) Yang, Z.; Qin, S.; Ye, X.; Liu, Z.; Guo, Y.; Cui, H.; Ge, J.-y. Y.; Li, H.; Long, Y.; Zeng, Y. J. Large magnetic entropy change in weberite-type oxides Gd_3MO_7 (M = Nb, Sb, and Ta). *Sci. China: Phys., Mech. Astron.* **2022**, *65*, 247011.
(42) Palacios, E.; Rodríguez-Velamazán, J. A.; Evangelisti, M.; McIntyre, G. J.; Lorusso, G.; Visser, D.; de Jongh, L. J.; Boatner, L. A. Magnetic structure and magnetocalorics of $GdPO_4$. *Phys. Rev. B: Condens. Matter Mater. Phys.* **2014**, *90*, 214423.
(43) Palacios, E.; Evangelisti, M.; Sáez-Puche, R.; Dos Santos-García, A. J.; Fernández-Martínez, F.; Cascales, C.; Castro, M.; Burriel, R.; Fabelo, O.; Rodríguez-Velamazán, J. A. Magnetic structures and magnetocaloric effect in RVO_4(R=Gd, Nd). *Phys. Rev. B* **2018**, *97*, 214401.
(44) Chogondahalli Muniraju, N. K.; Baral, R.; Tian, Y.; Li, R.; Poudel, N.; Gofryk, K.; Barišić, N.; Kiefer, B.; Ross, J. H.; Nair, H. S. Magnetocaloric Effect in a Frustrated Gd-Garnet with No Long-Range Magnetic Order. *Inorg. Chem.* **2020**, *59*, 15144.
(45) Kleinhans, M.; Eibensteiner, K.; Leiner, J. C.; Spallek, J.; Regnat, A.; Pfleiderer, C. Magnetocaloric properties of $(RE)_3Ga_5O_{12}$ (RE= Tb, Gd, Nd, Dy). *Phys. Rev. Appl.* **2023**, *19*, 014038.
(46) Wood, M. E.; Potter, W. H. General analysis of magnetic refrigeration and its optimization using a new concept: maximization of refrigerant capacity. *Cryogenics* **1985**, *25*, 667.
(47) Lorusso, G.; Sharples, J. W.; Palacios, E.; Roubeau, O.; Brechin, E. K.; Sessoli, R.; Rossin, A.; Tuna, F.; McInnes, E. J.; Collison, D.; Evangelisti, M. A dense metal-organic framework for enhanced magnetic refrigeration. *Adv. Mater.* **2013**, *25*, 4653.
(48) Yang, Z.; Zhang, H.; Bai, M.; Li, W.; Huang, S.; Ruan, S.; Zeng, Y.-J. Large magnetocaloric effect in gadolinium borotungstate Gd_3BWO_9. *J. Mater. Chem. C* **2020**, *8*, 11866.
(49) Roy, S.; Khan, N.; Mandal, P. Giant low-field magnetocaloric effect in single-crystalline $EuTi_{0.85}Nb_{0.15}O_3$. *APL Mater.* **2016**, *4*, 026102.
(50) Palacios, E.; Tomasi, C.; Sáez-Puche, R.; Dos santos-García, A. J.; Fernández-Martínez, F.; Burriel, R. Effect of Gd polarization on the large magnetocaloric effect of $GdCrO_4$ in a broad temperature range. *Phys. Rev. B* **2016**, *93*, 064420.
(51) Midya, A.; Khan, N.; Bhoi, D.; Mandal, P. 3d-4f spin interaction induced giant magnetocaloric effect in zircon-type $DyCrO_4$ and $HoCrO_4$ compounds. *Appl. Phys. Lett.* **2013**, *103*, 092402.
(52) Meng, L.; Jia, Y.; Li, L. Large reversible magnetocaloric effect in the $RECoC_2$ (RE=Ho and Er) compounds. *Intermetallics* **2017**, *85*, 69.
(53) Zhang, Y.; Zhu, J.; Li, S.; Zhang, Z.; Wang, J.; Ren, Z. Magnetic properties and promising magnetocaloric performances in the antiferromagnetic $GdFe_2Si_2$ compound. *Sci. China Mater.* **2022**, *65*, 1345.
(54) Xu, Q.; Liu, B.; Ye, M.; Zhuang, G.; Long, L.; Zheng, L. $Gd(OH)F_2$: A Promising Cryogenic Magnetic Refrigerant. *J. Am. Chem. Soc.* **2022**, *144*, 13787.
(55) Mukherjee, P.; Wu, Y.; Lampronti, G.; Dutton, S. Magnetic properties of monoclinic lanthanide orthoborates, $LnBO_3$, Ln= Gd, Tb, Dy, Ho, Er, Yb. *Mater. Res. Bull.* **2018**, *98*, 173.
(56) Mahana, S.; Manju, U.; Topwal, D. $GdCrO_3$: a potential candidate for low temperature magnetic refrigeration. *J. Phys. D: Appl. Phys.* **2018**, *51*, 305002.
(57) Das, M.; Roy, S.; Khan, N.; Mandal, P. Giant magnetocaloric effect in an exchange-frustrated $GdCrTiO_5$ antiferromagnet. *Phys. Rev. B* **2018**, *98*, 104420.
(58) Mahana, S.; Manju, U.; Topwal, D. Giant magnetocaloric effect in $GdAlO_3$ and a comparative study with $GdMnO_3$. *J. Phys. D: Appl. Phys.* **2017**, *50*, 035002.
(59) Dey, K.; Indra, A.; Majumdar, S.; Giri, S. Cryogenic magnetocaloric effect in zircon-type RVO_4 (R = Gd, Ho, Er, and Yb). *J. Mater. Chem. C* **2017**, *5*, 1646.
(60) Das, M.; Roy, S.; Mandal, P. Giant reversible magnetocaloric effect in a multiferroic $GdFeO_3$ single crystal. *Phys. Rev. B* **2017**, *96*, 174405.
(61) Midya, A.; Mandal, P.; Rubi, K.; Chen, R.; Wang, J.-S.; Mahendiran, R.; Lorusso, G.; Evangelisti, M. Large adiabatic temperature and magnetic entropy changes in $EuTiO_3$. *Phys. Rev. B* **2016**, *93*, 094422.
(62) Yang, Y.; Zhang, Q.-C.; Pan, Y.-Y.; Long, L.-S.; Zheng, L.-S. Magnetocaloric effect and thermal conductivity of $Gd(OH)_3$ and $Gd_2O(OH)_4(H_2O)_2$. *Chem. Commun.* **2015**, *51*, 7317.
(63) Krishna Murthy, J.; Devi Chandrasekhar, K.; Mahana, S.; Topwal, D.; Venimadhav, A. Giant magnetocaloric effect in Gd2NiMnO6and Gd2CoMnO6ferromagnetic insulators. *J. Phys. D: Appl. Phys.* **2015**, *48*, 355001.
(64) Chen, Y.-C.; Qin, L.; Meng, Z.-S.; Yang, D.-F.; Wu, C.; Fu, Z.; Zheng, Y.-Z.; Liu, J.-L.; Tarasenko, R.; Orendáč, M.; Prokleška, J.; Sechovský, V.; Tong, M.-L. Study of a magnetic-cooling material $Gd(OH)CO_3$. *J. Mater. Chem. A* **2014**, *2*, 9851.
(65) Midya, A.; Khan, N.; Bhoi, D.; Mandal, P. Giant magnetocaloric effect in magnetically frustrated $EuHo_2O_4$ and $EuDy_2O_4$ compounds. *Appl. Phys. Lett.* **2012**, *101*, 132415.

https://doi.org/10.1021/acs.inorgchem.3c00421
Inorg. Chem. 2023, 62, 5282−5291

(66) Han, Y.; Han, S.-D.; Pan, J.; Ma, Y.-J.; Wang, G.-M. An excellent cryogenic magnetic cooler: magnetic and magnetocaloric study of an inorganic frame material. *Mater. Chem. Front.* **2018**, *2*, 2327.
(67) Han, S.-D.; Miao, X.-H.; Liu, S.-J.; Bu, X.-H. Magnetocaloric effect and slow magnetic relaxation in two dense (3,12)-connected lanthanide complexes. *Inorg. Chem. Front.* **2014**, *1*, 549.
(68) Yang, Z.; Ge, J.-Y.; Ruan, S.; Cui, H.; Zeng, Y.-J. Cryogenic magnetocaloric effect in distorted double-perovskite Gd_2ZnTiO_6. *J. Mater. Chem. C* **2021**, *9*, 6754.
(69) Mukherjee, P.; Sackville Hamilton, A. C.; Glass, H. F. J.; Dutton, S. E. Sensitivity of magnetic properties to chemical pressure in lanthanide garnets $Ln_3A_2X_3O_{12}$, Ln = Gd, Tb, Dy, Ho, A = Ga, Sc, In, Te, X = Ga, Al, Li. *J. Phys.: Condens. Matter* **2017**, *29*, 405808.
(70) Stanley, H. E. Scaling, universality, and renormalization: Three pillars of modern critical phenomena. *Rev. Mod. Phys.* **1999**, *71*, S358.
(71) Franco, V.; Conde, A. Scaling laws for the magnetocaloric effect in second order phase transitions: From physics to applications for the characterization of materials. *Int. J. Refrig.* **2010**, *33*, 465.
(72) Shen, T. D.; Schwarz, R. B.; Coulter, J. Y.; Thompson, J. D. Magnetocaloric effect in bulk amorphous $Pd_{40}Ni_{22.5}Fe_{17.5}P_{20}$ alloy. *J. Appl. Phys.* **2002**, *91*, 5240.
(73) Law, J. Y.; Franco, V.; Moreno-Ramírez, L. M.; Conde, A.; Karpenkov, D. Y.; Radulov, I.; Skokov, K. P.; Gutfleisch, O. A quantitative criterion for determining the order of magnetic phase transitions using the magnetocaloric effect. *Nat. Commun.* **2018**, *9*, 2680.
(74) Franco, V.; Conde, A.; Romero-Enrique, J. M.; Blázquez, J. S. A universal curve for the magnetocaloric effect: an analysis based on scaling relations. *J. Phys.: Condens. Matter* **2008**, *20*, 285207.
(75) Zeleňáková, A.; Hrubovčák, P.; Kapusta, O.; Zeleňák, V.; Franco, V. Large magnetocaloric effect in fine Gd_2O_3 nanoparticles embedded in porous silica matrix. *Appl. Phys. Lett.* **2016**, *109*, 122412.

https://doi.org/10.1021/acs.inorgchem.3c00421
Inorg. Chem. 2023, 62, 5282−5291